Data Repository Item 2017393

Cosmogenic exposure ages indicate that periglacial boulder fields are ancient, multigenerational features

Alison R. Denn, Paul R. Bierman, Susan R. H. Zimmerman, and Mark W. Caffee, Lee B. Corbett, and Eric Kirby

Contents:

DR Figures:

DR Tables:

1. Semivariogram and spatial autocorrelation of boulders

Semivariance is a spatial statistic that measures the dissimilarity between measurements over a distance. Semivariance is defined by the equation:

$$\gamma(h) = \frac{1}{2N(h)} \sum_{i=1}^{N(h)} [u(a)_i - u(a+h)_i]^2 \qquad \text{(Eq. 1)}$$

Where $\gamma(h)$ is the semivariance, $N(h)$ is the total number of sample pairs separated by a distance h, and $u(a)$ and $u(a+h)$ are the locations of a sample pair separated by h (Isaaks and Srivastava, 1989; Portenga et al., 2013).

To create the semivariogram plot (A), we calculated the semivariance and distance between every possible pair of ^{10}Be measurements from the main boulder field. Semivariance is plotted on the y axis and lag distance (*h*) is plotted on the x axis. To create the experimental semivariogram (B), we divided the semivariogram into 50 m bins and plotted the average $\gamma(h)$ of each bin with 95% confidence interval. The third diagram is the model semivariogram (C), in which an exponential model is fit through the points. The γ(h) value and the (*h*) value at which the model flattens out are called the 'sill' and 'range' respectively, and represent the point at which samples are no longer spatially autocorrelated. The model does not pass through the origin, it is projected to a point on the γ(h) axis >0. This discrepancy is caused by the inherent error in sample collection and measurement (Journel and Huijbregts, 1978).

The model semivariogram shown here has a sill of 1.25 x 10^{12}, a range of 450 m, and a nugget of 0.1 x 10^{12} (C). The range marks the point at which the consistent increase in $\gamma(h)$ ends. The model semivariogram demonstrates that the concentration of ^{10}Be in boulders becomes increasingly different over the length of the field.

2. Boulder HR10 flipping and burial calculations

Cosmogenic nuclide production decreases exponentially with depth at Earth's surface according to the equation:

$$P(x) = P(0)e^{-(\rho x/\Lambda)} \qquad \text{(Eq. 2)}$$

Where x is the depth (cm), ρ is the density (we assume 2.7 g/cm^3), Λ is the absorption mean free path for nuclear particles in the rock (with an assumed value of 160 g/cm^2), and *P*(0) is the production rate of the cosmogenic nuclide at the rock surface (Nishiizumi et al., 1991).

We sampled on the top (HR10T), bottom (HR10B), and clasts underneath (HR10C1-3) boulder HR10 in order to test whether ^{10}Be concentrations were consistent with continuous exposure in place. To do this, we solved Eq. 2 for the production rate at depth, assuming a surface production rate of 5.9 atoms *$g^{-1}yr^{-1}$from the CRONUS exposure calculator using the northeastern United States production rate calibration dataset (Balco et al., 2009), using version wrapper script 2.2, main calculator 2.1, constants 2.2.1, (http://hess.ess.washington.edu/, see Balco et al. (2008)). We multiplied the percentage of the surface production rate by the measured concentration in HR10T to calculate the expected ^{10}Be concentration for each subsurface sample. The modeled concentrations were an order of magnitude lower than the measured values, confirming that boulder HR10 and the underlying clasts could not have been continuously exposed in their present geometry.

After ruling out continuous exposure in place, we created a simple model in which the boulder flipped at 25 ka (the LGM). We subtracted 25 ka worth of ^{10}Be production from each sample using the production rate at each respective depth and made a new production curve, setting sample HR10B as the 'top' at 25 ka. Sample HR10 plots far to the right of this curve and has too much ^{10}Be to have been exposed as recently as 25 ka. When we repeat this exercise by subtracting 200 ka of exposure (the beginning of MIS 6, the Illinoian glacial period) HR10B and HR10T align, consistent with a boulder flip at 200 ka. The clasts, on the other hand, have concentrations that are high on both curves, suggesting that boulder HR10 has not always shielded the clasts.

Our third model was to test whether the $^{26}Al/^{10}Be$ ratios in the clasts would have been significantly altered by 200 ka of burial under boulder HR10. Nuclides decay according to:

$$\frac{N_{26}}{N_{10}} = \left(\frac{N_{26}}{N_{10}}\right)_0 e^{-t_{burial}(1/\tau_{26} - 1/\tau_{10})} \qquad \text{(Eq.3)}$$

We assumed that at time zero, after the flip, that the clasts had a concentration of ^{26}Al and ^{10}Be at a ratio of 7. For each century, we added in 100 years of nuclide production at 0.65 m depth and subtracted a 100 years of decay. We repeated this process for 200 ka. The resultant concentration still plots within 2 σ of the surface production ratio.

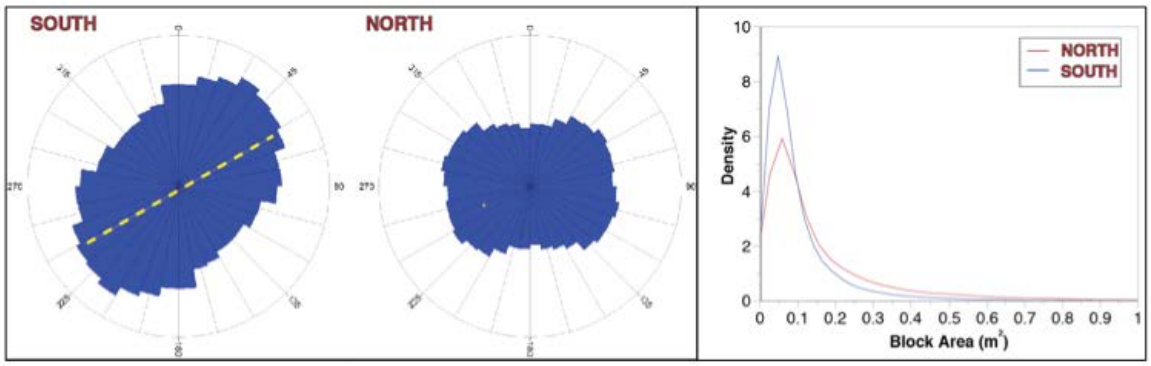

Figure DR1: Results of image analysis. The orientation of blocks in the northern imagery is E-W, whereas southern blocks follow the trend of the main axis of the field (dotted yellow line). Block size is similarly distributed in both areas; modal block size (~0.03 m^2) is the same in both swaths of imagery. However, there is a statistically significant decrease in mean block size between the two. Average block size in the north is 0.16 m^2, whereas block size in the south is 0.11m^2 because there is a long tail of large blocks in the north.

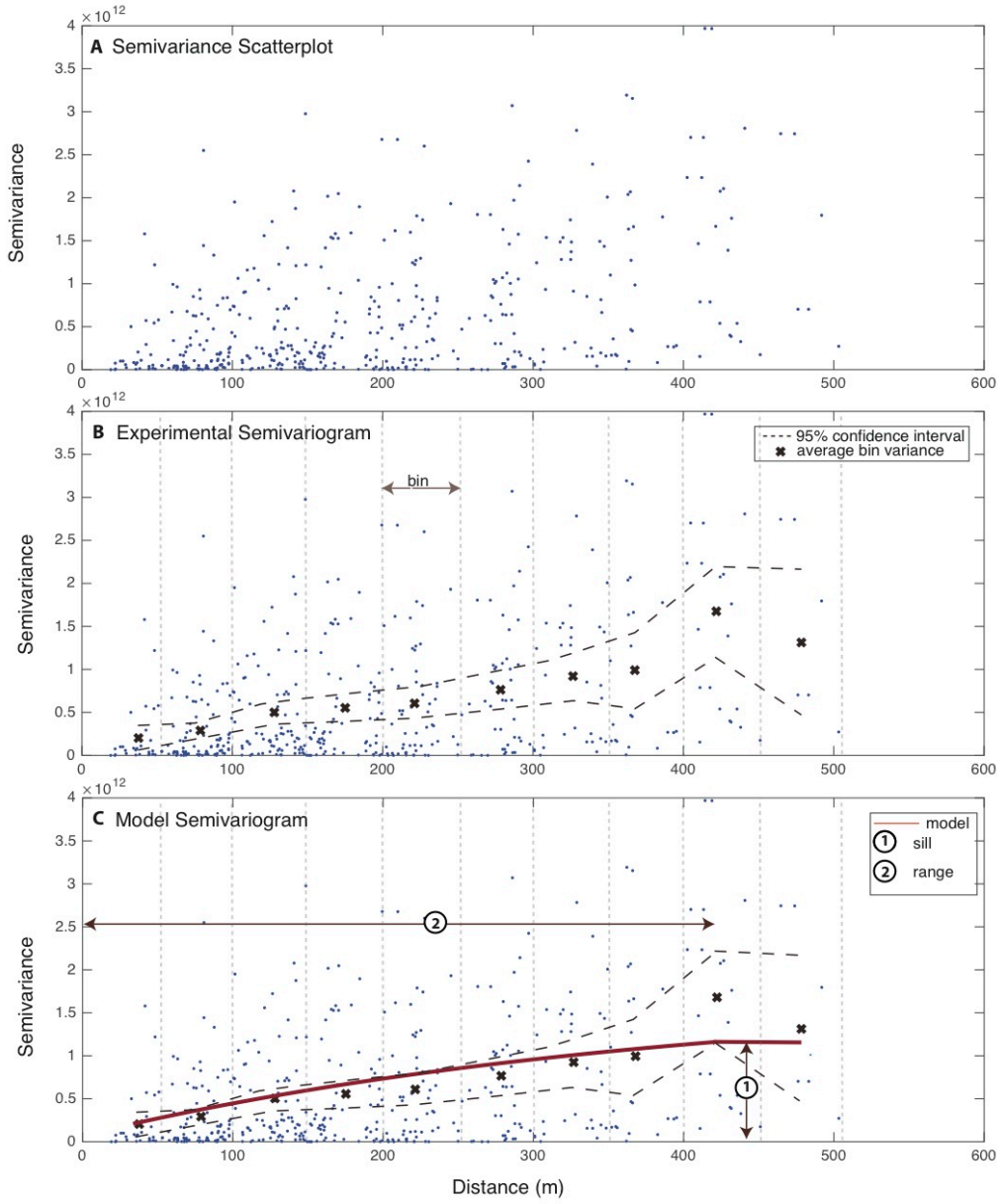

Figure DR2: Semivariogram of ^{10}Be measurements in boulders from the main field at Hickory Run. (A) Semivariance scatterplot, each point represents the calculated semivariance and distance between a boulder pair. Every permutation of two boulders from the main field is plotted. (B) Experimental semivariogram of the field, measurements are binned every 50 m and plotted with 95% confidence interval. (C) Model fit of the experimental semivariogram. Spatial autocorrelation ends between 400-500 m; boulders have increasingly different concentrations over the length of the field.

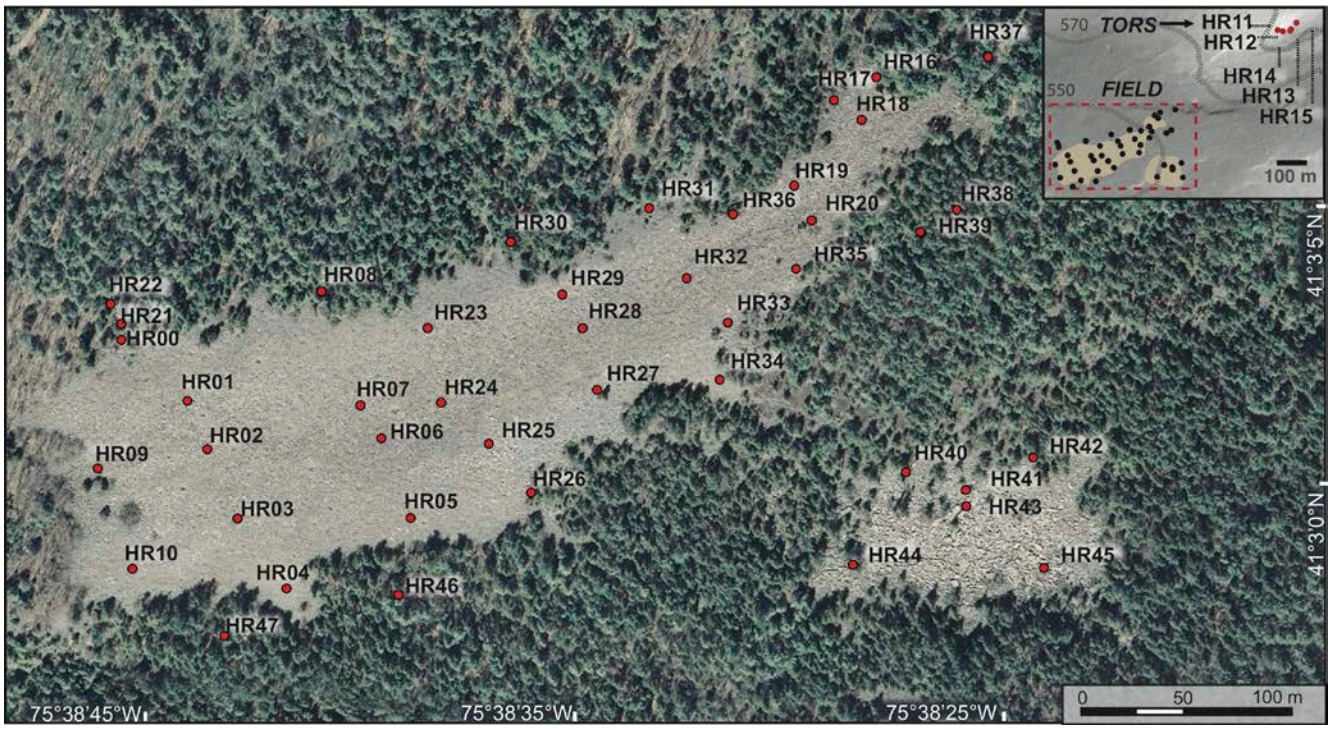

Figure DR3: Hickory Run sampling location map by name.

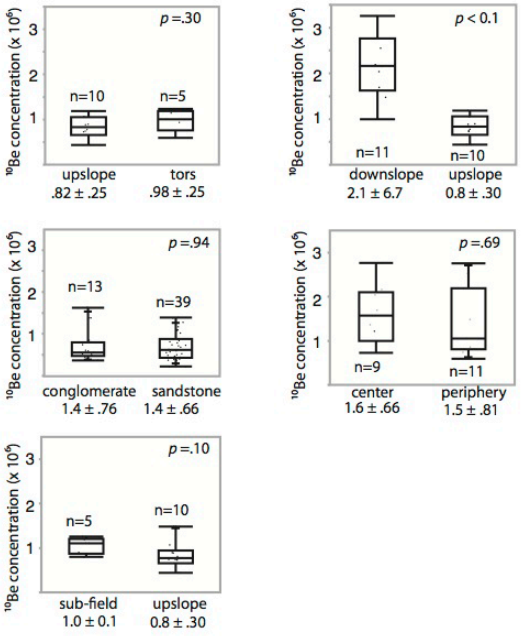

Figure DR4: Box and whiskers plots of boulder types, comparisons made using Student's *t*-test. The ends of the whiskers represent the range of ^{10}Be concentrations,

while the top, middle, and bottom of each box mark the 75th, 50th, and 25th percentiles.

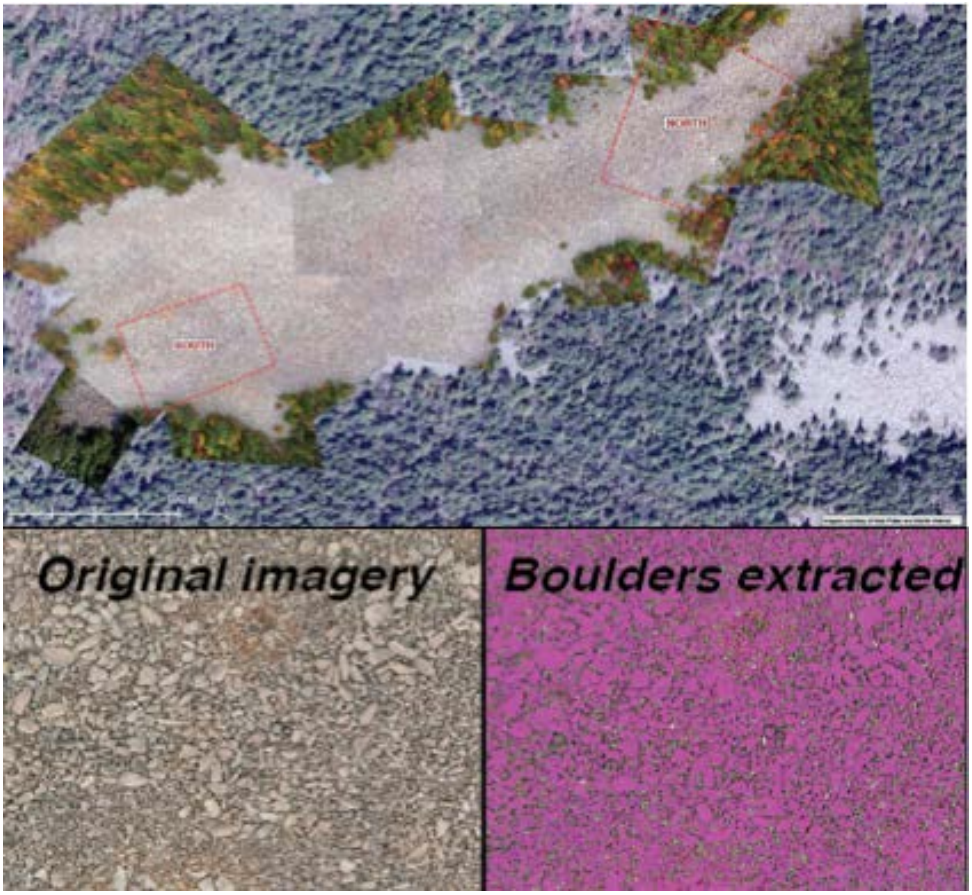

Figure DR5: Dotted red boxes mark the location of the northern and southern swaths of high resolution aerial imagery analyzed (above) and visual representation of how eCognition software extracts boulders (below). Our ruleset automatically exports information about the size and orientation of each feature.

References

Isaaks, E. H., and Srivastava, R. M., 1989, Applied geostatistics: Oxford University Press: New York, p. 561.

Journel, A. G., and Huijbregts, C. J., 1978, Mining geostatistics, Academic press.

Nishiizumi, K., Kohl, C. P., Arnold, J. R., Klein, J., Fink, D., and Middleton, R., 1991, Cosmic ray produced ^{10}Be and ^{26}Al in Antarctic rocks; exposure and erosion history: Earth and Planetary Science Letters, v. 104, no. 2-4, p. 440-454.

Portenga, E. W., Bierman, P. R., Rizzo, D. M., and Rood, D. H., 2013, Low rates of bedrock outcrop erosion in the central Appalachian Mountains inferred from *in situ* ^{10}Be concentrations: Geological Society of America Bulletin, v. 125, no. 1-2, p. 201-215.